Multi-Stimuli-Responsive and Mechano-Actuated Biomimetic Membrane Nanopores Self-Assembled from DNA

Yongzheng Xing,* Adam Dorey, and Stefan Howorka*

In bioinspired design, biological templates are mimicked in structure and function by highly controllable synthetic means. Of interest are static barrel-like nanopores that enable molecular transport across membranes for use in biosensing, sequencing, and biotechnology. However, biological ion channels offer additional functions such as dynamic changes of the entire pore shape between open and closed states, and triggering of dynamic processes with biochemical and physical stimuli. To better capture this complexity, this report presents multi-stimuli and mechano-responsive biomimetic nanopores which are created with DNA nanotechnology. The nanopores switch between open and closed states, whereby specific binding of DNA and protein molecules as stimuli locks the pores in the open state. Furthermore, the physical stimulus of high transmembrane voltage switches the pores into a closed state. In addition, the pore diameters are larger and more tunable than those of natural templates. These multi-stimuli-responsive and mechanically actuated nanopores mimic several aspects of complex biological channels yet offer easier control over pore size, shape and stimulus response. The designer pores are expected to be applied in biosensing and synthetic biology.

1. Introduction

Biological membrane nanopores and ion channels are functionally important conduits for transport of molecular cargo across lipid bilayer membranes. In the simplest form, structurally static barrel-like nanopores are constitutively open for water-soluble cargo small enough to pass the pore lumen. Natural ion channels are structurally and functionally more complex by undergoing conformational changes that control transport, and also by harboring a selectivity filter for permitted molecules. To gate transport, the ion channels switch between open and closed states that represent mechanical changes in channel shape and lumen. These hallmark changes are triggered by environmental stimuli such as ligand binding,[1–3] voltage,[4–7] membrane torsion,[8–10] and mechanical forces.[11,12] In highly complex channels, conformational flexibility is coupled with multi-step activation to tightly control channel lumen width and transport.[13]

Engineering biological and fabricating completely new synthetic nanopores is relevant to tune pore shape and function for biosensing, biotechnology, and synthetic biology. For example, protein pores were engineered for widely used next-generation portable DNA sequencing[14–18] and label-free electrical biosensing.[19–33] In the sensing principle, individual analyte molecules pass through the electrolyte-filled pore and can thereby cause transient detectable changes in the electrical readout. To provide a low-noise signal, the pores are ideally structurally stable and do not undergo any conformational changes. By comparison, designing nanopores to undergo controlled conformational opening and closing offers a route to functionally more complex and high-value devices for sensing and synthetic biology. De-novo design with synthetic approaches[34] can rely on organic-polymeric materials[32] and also peptide scaffolds.[35–40] While the synthetic scope is impressive, these approaches have some limitations, such as the challenge to design controlled conformational changes. Furthermore, the approaches yield only small lumen sizes of a few nanometer that restrict applications to non-protein transport. To better mimic biology and expand the application range, future synthetic pores should achieve stimulus-responsiveness coupled with nanomechanical actuation of pore shape and lumen. Ideally, the pores should also have wider and tunable lumens. Pores with >5 nm inner width are of general interest as they can accommodate large proteins or protein complexes for direct sensing at the single-molecule level.[41] Wide pores may also be used in synthetic biology for controlling transport of large biomolecular cargo across membranes.[42]

Y. Xing, A. Dorey, S. Howorka
Department of Chemistry & Institute of Structural and Molecular Biology
University College London
20 Gordon Street, London WC1H 0AJ, UK
E-mail: y.xing@ucl.ac.uk; s.howorka@ucl.ac.uk

**ADVANCED
SCIENCE NEWS**
www.advancedsciencenews.com

**ADVANCED
MATERIALS**
www.advmat.de
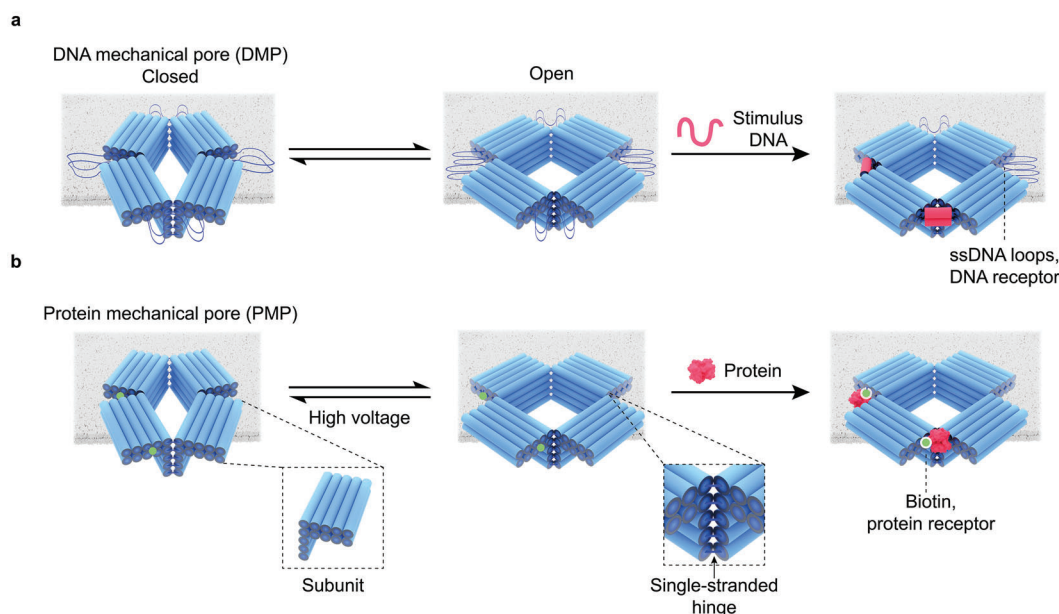
Scheme 1. Design and functional principle of self-assembled DNA-made mechanical nanopores. a) Illustration of a DNA-binding mechanical pore (DMP) showing rapid fluctuations between a closed state (left) and open state (middle). Sequence-specific binding of stimuli DNA strands (red) forms pairs of DNA duplexes at two corners that stabilize the pore structure in an open configuration (right). b) The protein-binding mechanical pore (PMP) also undergoes dynamic fluctuations. A high transmembrane potential switches the pore into the closed state. Binding of two streptavidin protein molecules (red) to biotin tags (green) at adjacent corners of PMP stabilizes the structure in an open conformation (right).

Here, we develop synthetic nanopores that undergo conformational transitions that are triggered by biomolecular and physical stimuli, and offers up to >10 nm-wide lumens. The rational design of the synthetic nanopores is realized with DNA nanotechnology[43–46] that is a powerful tool to build well-defined nanostructures of customized dimension and shape,[47–50] structural curvature,[51,52] mechanical properties,[53–57] and designable functionalization.[46,58,59] Recently, DNA membrane nanopores[41,60–66] have been fabricated and functionalized with hydrophobic moieties for membrane insertion. However, these existing DNA pores did not feature any designed changes in pore lumen shape even though some were equipped with flap-like gates responding to triggers.[42,62,67–69] Our nanopores presented here undergo dynamic conformational transitions between open and closed states (**Scheme 1**). According to our designable control mechanism, the semiflexible pores can be mechanically locked in the open state by specific recognition of biomolecular stimuli or can be switched to the closed state upon application of a high transmembrane voltage (Scheme 1). Notably, the pores have a diameter of >10 nm, which is otherwise challenging to achieve via de novo building routes with proteins. Our multi-stimuli-responsive and mechanically actuated nanopores mimic many aspects of complex biological ion channels yet offer easier tuning over pore size, shape and stimulus response. We expect the designer DNA pores to be applied in biosensing and synthetic biology.

2. Results and Discussion

The design of our mechanical nanopores with stimulus-controlled shape and rigidity was enabled by DNA nanotechnology. As shown in Scheme 1, the semiflexible DNA-origami nanopore features four structurally stable subunits composed of bundled DNA duplexes. Flexibility is introduced as the modular subunits are interconnected with single-stranded DNA (ssDNA) hinges at their innermost duplexes (Scheme 1). Given the lack of stabilization at the corners, the entire structure spontaneously fluctuates between a rhombus and a square shape (Scheme 1), as implied by its name, mechanical pore MP.

To confer the pore with tunable structural rigidity in response to biomolecular stimuli, two design routes were devised (Scheme 1, Figures S1 and S2, Supporting Information). In the first, DNA stimuli control the DNA-binding mechanical pore DMP. The pore's rigidity is tunable as its subunits are interlinked with ssDNA loops that hybridize with stimuli DNA strands to form duplexes that stabilize the pore in the open state (Scheme 1a). The second design is analogous but uses protein as trigger, whereby the protein-binding mechanical pore (PMP) carries at its corners protein-binding receptors (e.g., biotin moieties, Scheme 1b). After specific binding, the bulky target proteins (e.g., streptavidin) sterically occupy the corners and force the mechanical nanopore to adopt an open conformation. To gain fine control of the pore structures, up to four of the
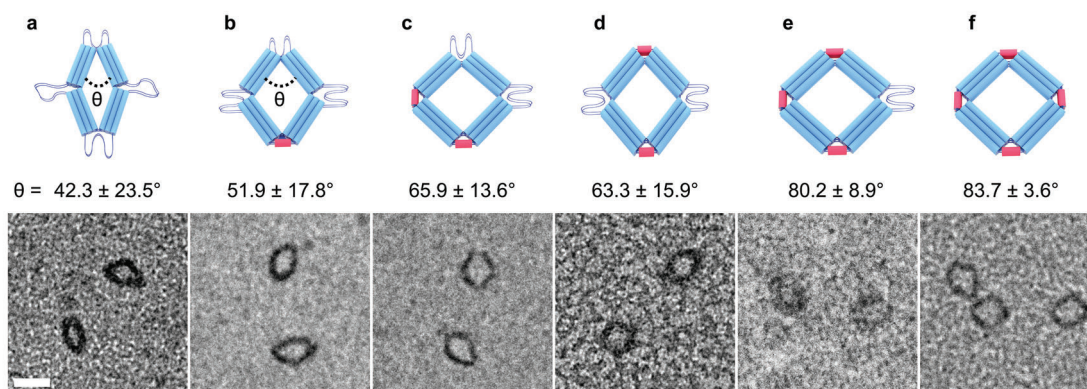
Figure 1. a–f) Schematic representations (top) and TEM images (bottom) of DNA-binding mechanical cap (DMC) structures, from left to right: a) without stabilizing DNA duplexes (DMC-0), b) with one pair (DMC-1), c) two pairs at adjacent corners (DMC-2) or d) diagonal corners (DMC-2d), e) three pairs (DMC-3), and f) four pairs (DMC-4) of stabilizing duplexes, respectively. Scale bar: 20 nm.

corners can be targeted by the DNA or protein stimuli leading to a progressively more opened pore lumen. For example, the DNA-responsive pore shown in Scheme 1a carries two pairs of stabilizing DNA duplexes at two adjacent corners while the protein-responsive variant is functionalized with two biotin tags and bound with two proteins (Scheme 1b). In another type of mechanical control, the physical stimulus of transmembrane voltage with high magnitude causes controlled closing of the semiflexible pore (Scheme 1b). The mechanism is based on the negatively charged nature of the backbone of the DNA strands in the DNA nanopore. Under applied transmembrane voltage, some of these strands may undergo limited electrophoretic movement and alter the fine structure of the pore.[70,71] This process usually increases with voltage. Additionally, lateral membrane pressure may influence open and closed states of membrane-inserted nanopores.

2.1. DNA-Binding Mechanical Nanopores

To verify the principle of tunable rigidity, we first fabricated a series of DNA-triggered mechanical cap (DMC) structures that can bind stabilizing oligonucleotide strands at tunable numbers and corner positions. We used a design with two duplex layers in each subunit because it has higher rigidity within the subunit compared to a single-layered design. Up to six structures were constructed (**Figure 1**) including caps without stabilizing DNA duplexes (DMC-0), with one pair (DMC-1), two pairs at adjacent corners (DMC-2) or diagonal corners (DMC-2d), three pairs (DMC-3), and four pairs (DMC-4) of stabilizing duplexes, respectively. The DNA-origami structures of 20 nm-long subunits were self-assembled by mixing 20 nM pre-treated M13 scaffold and five times excess staples (Table S1, Supporting Information) in 0.5x TAE buffer supplemented with 16 mM $MgCl_2$ and folding by using a 40 h annealing program. The folded samples were analyzed with 1.5% agarose gel electrophoresis (Figure S3a, Supporting Information), and the defined bands suggest that the structures were folded efficiently. The DMC samples were then purified with 1.2% agarose gel electrophoresis for analysis with trans-

mission electron microscopy (TEM). TEM images (Figure 1; Figure S4, Supporting Information) showed that the six DMC structures were successfully formed.

To obtain an understanding of how the number and position of the stabilizing duplexes influenced the constructs' rigidity, TEM images were analyzed to obtain the small angle, θ, of the rhombus-shaped lumens (Figure 1a). The value of θ for DMC-0 was 42.3 ± 23.5, indicating a flexible structure, while an increase in the number of stabilizing duplexes led to gradually higher θ. The values were 51.9 ± 17.8, 65.9 ± 13.6, 63.3 ± 15.9, 80.2 ± 8.9, and 83.7 ± 3.6 ($n \geq 35$) for DMC-1, DMC-2, DMC-2d, DMC-3, and DMC-4, respectively (Figure 1 and Table S2, Supporting Information). The standard deviation of θ decreased, however, in the series. The trend of the increasing average angles suggests a higher degree of opening for the structures while the deceasing angle deviations indicate higher structural rigidities and thus more stable conformations.

After validating the DNA-stabilizing principle, we next designed and built DNA-binding mechanical pore (DMP) nanostructures (Scheme 1 and **Figure 2**). In DMP, the cap subunits had a length of 10 nm. Compared to DMC, the subunits were horizontally broadened from three to five duplexes to help accommodate a sufficiently high number of cholesterol tags for membrane anchoring.[41] As other change, the underside of the DMP subunits featured a four duplex-high transmembrane tip to puncture the bilayer. The DMP structures were folded with the phiX174 scaffold and corresponding staples (Table S1, Supporting Information) by using the same folding procedures to the DMC structures, followed by agarose gel electrophoresis to confirm the efficient folding (Figure S3b, Supporting Information) and gel purification for use of further experiments.

To establish that the DMP pores span lipid membrane bilayers and to characterize the biophysical differences between pore conformations, single-channel current recordings were performed. This technique uses an applied transmembrane voltage to induce the detectable flow of solubilized ions through a membrane puncturing channel. Nanomechanical pores designed for DNA response were analyzed in two versions: DMP-0 without
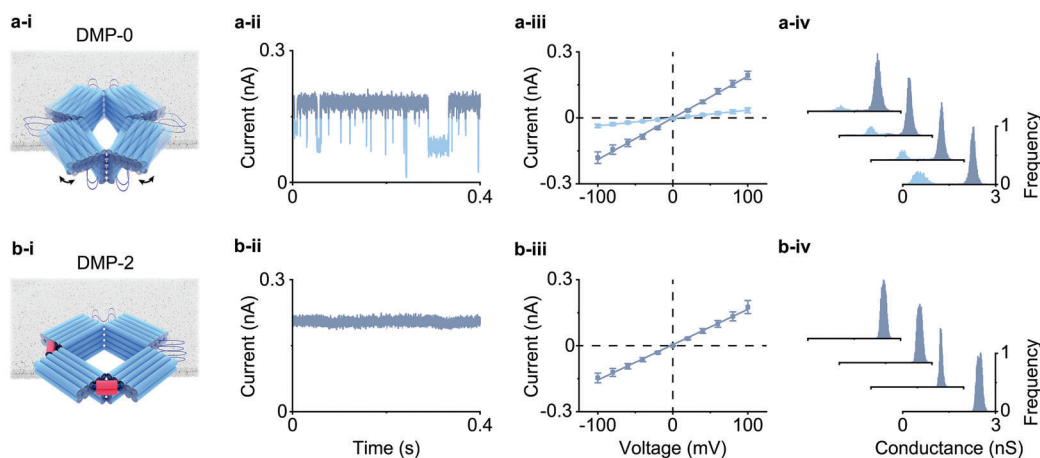
2300589 (3 of 9)

Figure 2. Electrical characterization of DNA-binding mechanical pore (DMP) structures with DNA-triggered transition from a dynamic fluctuating to an open state. a,b) Electrical recording analysis of DMP-0 without stabilizing duplex (a) and DMP-2 with two pairs of stabilizing duplexes at adjacent corners (b). i) Schematic representation of the DMP structures. ii) Single-channel current traces obtained at +80 mV. iii) Average current–voltage plots (± s.e.m.) for voltages ranging from −100 to +100 mV at 20 mV steps. iv) All-point histogram of channel conductances at +80 mV. In (ii)–(iv), the closed state is indicated by light blue and the open state by dark blue.

stabilizing duplexes and DMP-2 for binding DNA at two adjacent corners (Figure 2). The two pores were analyzed under the standard electrolyte solution of 1 M KCl, 10 mM HEPES pH 7.4 using a transmembrane potential of up to +100 or −100 mV to induce the electrophoretic flow of ions as measured by ionic current. Insertion of large DNA-origami structures into lipid membranes is not an energetically favorable process due to the required displacement of lipid molecules to create a hole in the membrane. To improve insertion rates, pores were first modified to include cholesterol membrane anchors on the underside of the structure and second incubated with weak detergent (0.5% n-octyloligooxyethylene).[71] Characterization by single-channel current traces (Figure 2a-ii) revealed that DMP-0 pores exist in two states, open or closed, with the propensity to rapidly switch between these states (Figure S8, Supporting Information). Analyzing the current–voltage relationship (Figure 2a-iii) and all-point conductance histograms (Figure 2a-iv) revealed the closed state to have an average conductance of 0.36 ± 0.04 nS ($n = 9$, ± s.e.m.) and the open state a value of 1.95 ± 0.04 nS ($n = 8$). The nanopore's open state was stabilized by preincubation with binding DNA strands to form rigidified DMP-2 pores (Figure 2b). The successful transition was indicated in the current traces by the switch to the higher conductance state (Figure 2b-ii). Current–voltage relationships (Figure 2b-iii) and all-point conductance histograms (Figure 2b-iv) established that DMP-2 pores cluster only into the open pore state, with an average conductance of 1.79 ± 0.01 nS ($n = 15$) as expected for a pore stabilized in an open configuration. The magnitude was similar to the open state conductance of DMP-0 nanopores. Variation in conductance as shown by all-point conductance histograms (Figure 2b-iv) are in accordance with normal variation of similarly designed DNA nanopores.[41] Reducing the number of stabilizing duplexes to one (DMP-1) decreased the open pore conductance to 1.08 ± 0.03 nS ($n = 10$), whilst increasing the number of stabilizing du-

plexes to three (DMP-3) raised the open pore conductance to 2.48 ± 0.07 nS ($n = 5$), in line with a reduction and an increase in open pore area, respectively (Figure S9, Supporting Information).

2.2. Protein-Binding Mechanical Nanopores

To demonstrate protein-mediated stabilization, we designed and built protein-binding mechanical caps (PMC) before applying the principle to nanopores. Protein-responsive PMC was similar in overall structure to DMC but lacked the outer DNA-responsive ssDNA loops. However, PMC featured biotin functionalization at the corners to enable the binding of protein streptavidin leading to rigidification of the DNA structure (Scheme 1).

We prepared PMC structures without biotin (PMC-0), and modified versions with one (PMC-1) and two adjacent (PMC-2) biotin moieties, using folding and purification protocols used for the DMC structures. The successful self-assembly of PMC structures was confirmed with 1.5% agarose gel electrophoresis (Figure S5a, Supporting Information). To demonstrate specific protein-binding, the gel-purified nanostructures were incubated with streptavidin (PMC: streptavidin = 1: 300) for 1 h at room temperature. Analysis with 1.5% agarose gel electrophoresis demonstrated that the PMC-0 sample with streptavidin showed no band shift relative to the no protein control, while both the PMC-1 and PMC-2 constructs displayed slower band migration after incubated with streptavidin (**Figure 3**a; Figure S6a, Supporting Information). The data suggests the successful binding of streptavidin to the PMC-1 and PMC-2 structures. The PMC samples incubated with streptavidin were also imaged with TEM (Figure 3b; Figure S7, Supporting Information). The analysis of the small angle, θ, of the rhombus-shaped lumens was performed, and yielded values for PMC-0, PMC-1 and PMC-2 of 35.6 ± 31.9, 49.2 ± 22.3, and 56.1 ± 19.1, respectively ($n \geq 37$) (Table S3,
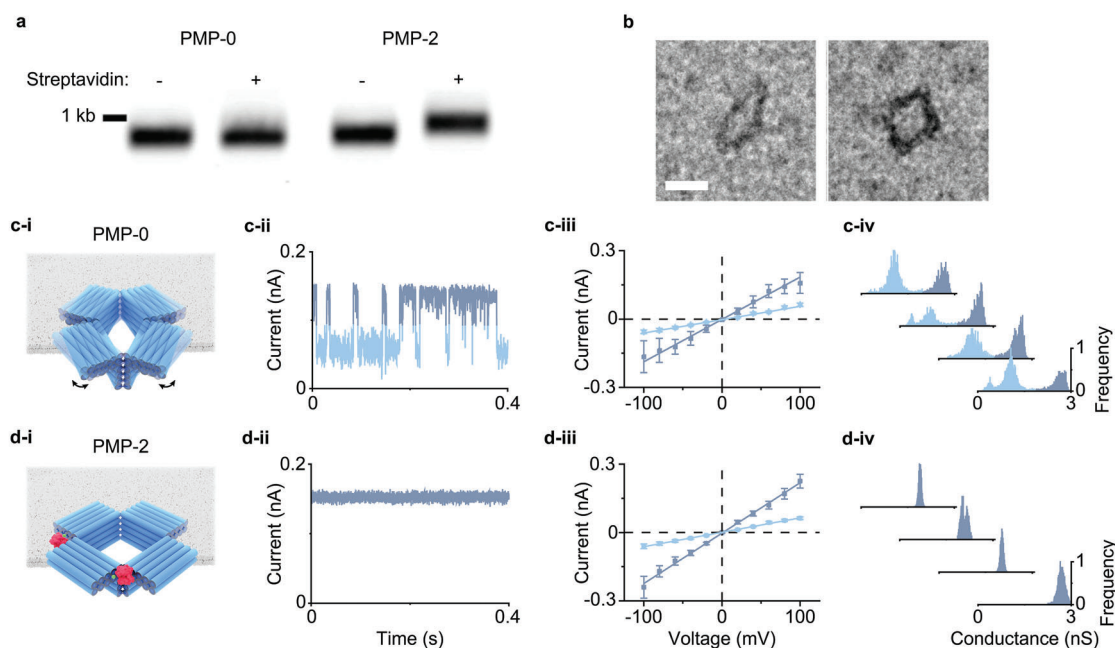
**ADVANCED
SCIENCE NEWS**

www.advancedsciencenews.com

**ADVANCED
MATERIALS**

www.advmat.de

Figure 3. Characterization of protein-binding mechanical caps and pores. a) 1.5% agarose gel electrophoresis of the protein-binding mechanical cap (PMC) structures without biotin modification (PMC-0), or functionalized with two biotin tags (PMC-2), incubated without or with streptavidin. b) TEM images showing PMC-0 and PMC-2 after incubation with streptavidin. Scale bar: 20 nm. c,d) Electrical recording analysis of protein-binding pores without biotin tags (PMP-0) and with two biotins (PMP-2) after pre-incubation with streptavidin. i) Schematic representation of the PMP structures. ii) Single-channelcurrent traces obtained at +80 mV. iii) Average current–voltage graphs (± s.e.m.) for voltages ranging from −100 to +100 mV at 20 mV steps. iv) All-point histogram of channel conductances at +80 mV. In (ii) to (iv), light blue indicates the closed state pore state and dark blue the open pore state.

Supporting Information). The increasing trend of θ demonstrates that binding of streptavidin to PMC-1 and PMC-2 structures can stabilize their rhombus-shaped lumens with more opened conformations than PMC-0. Furthermore, the angle standard deviations of the three PMCs are bigger compared with their DMC counterparts. The inferred higher structural flexibilities may be attributed to the lack of the outer ssDNA loops that otherwise provide extra stabilizing effects in the DMCs.

After establishing the stabilization principle, we designed and fabricated protein-binding mechanical pores (PMP) using 10 nm-long subunits with five-duplex wide caps and four duplex-high tips, analogous to the DMP pore. The protein-binding pores had zero (PMP-0), one (PMP-1), and two biotin tags (PMP-2), at the corners. After the programmed folding, the PMP structures were analyzed with 1.5% agarose gel electrophoresis (Figure S5b, Supporting Information) to verify that the structures had self-assembled efficiently. To confirm protein binding, the gel-purified pore structures were incubated with streptavidin and analyzed by agarose gel electrophoresis. Successful streptavidin binding was inferred from the band shifts of PMP-1 and PMP-2, compared with PMP-0 that showed no band shift (Figure S6b, Supporting Information).

To confirm that the protein-actuated pores are able to puncture lipid membrane bilayers, single-channel current recordings were performed. Protein-actuated pores PMP-0 and PMP-

2 were analyzed (Figure 3c,d) under the standard electrolyte solution. Characterization of current traces revealed that PMP-0 pores show similar characteristics to their DMP-0 counterparts, in terms of two states and the propensity to rapid switching between these states (Figure 3c-ii; Figure S8, Supporting Information). Current–voltage analysis (Figure 3c-iii) and conductance histogram (Figure 3c-iv) revealed that PMP-0 closed state had an average conductance of 0.59 ± 0.02 nS ($n = 11$) and the open state 1.86 ± 0.06 nS ($n = 6$). These values are concordant with DMP-0 conductances.

The open state of the biotin-modified pore PMP-2 was stabilized by incubation with streptavidin, as shown with electrical recordings. Following this analysis, protein-incubated PMP-2 clustered into two states, an open state and also a closed state (Figure S10, Supporting Information), unlike the single-state open DMP-2 pore. The dual state behavior of PMP-2 is likely a cause of incomplete binding of streptavidin to the DNA pore structure, potentially through partial inaccessibility of the biotin tags in the pore's corners. Analysis with current–voltage plots (Figure 3d-iii) and conductance histograms (Figure 3d-iv) revealed that the PMP-2's closed state had an average conductance of 0.64 ± 0.01 nS ($n = 8$), whilst the open state was at 2.81 ± 0.04 nS ($n = 12$). The open pore currents are higher than those of PMP-0 pores, suggesting that protein binding opens the pore lumen to a larger extent than in the fluctuations. A higher
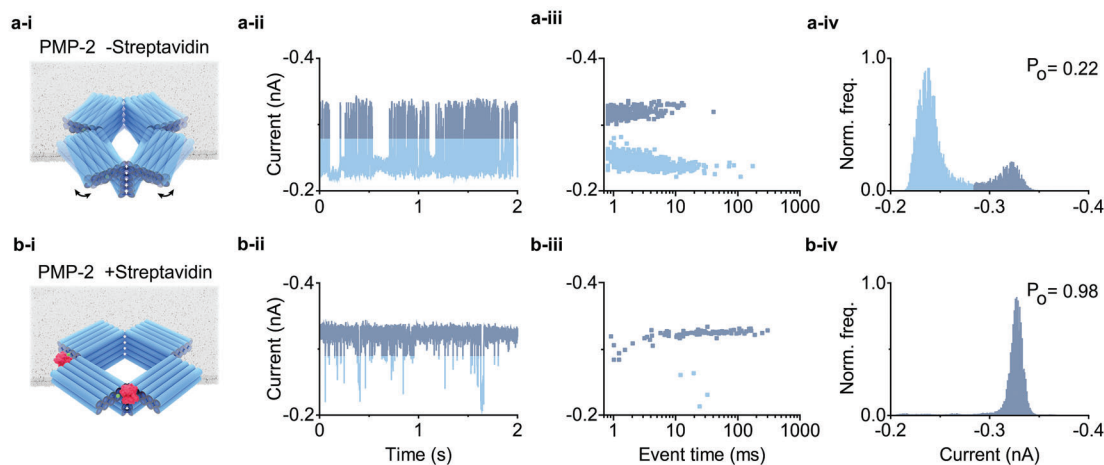
**ADVANCED
SCIENCE NEWS**

www.advancedsciencenews.com

**ADVANCED
MATERIALS**

www.advmat.de

Figure 4. Protein sensing with the protein-binding pore PMP-2. a) The PMP-2 pore prior to the addition of streptavidin. i) Schematic of the pore. ii) An example single-channel current trace at +80 mV shows rapid open and closing events in line with the structurally similar PMP-0 pore. iii) A scatter plot shows the fluctuations' distribution in current and duration. iv) An all-point conductance histogram reveals an open probability of 0.22. b) Analysis of the same pore after addition of 33 nM streptavidin to the cis chamber. i) Schematic drawing of the pore with two bound streptavidin molecules. ii) The single-channel current trace at +80 mV and iii) the scatter plot shows a reduction in rapid opening and closing events. iv) An all-point conductance histogram reveals a shift in the open probability to 0.98.

percentage of pores exists in the open state of PMP-2 (60%) in comparison to PMP-0 (35%), further confirming protein binding. Open pore conductances of PMP-2 are significantly higher than those of DMP-2, indicative of an increased pore area caused by protein binding in comparison to stabilization by DNA duplexes.

2.3. Protein-Binding Mechanical Pores as Sensing Devices

DNA nanopores have been used previously for sensing of proteins and other relevant bioanalytes.[65,41,42] We explored whether the nanomechanical pores are able to function as sensing devices. First, the unbound PMP-0 pore was used to determine whether pore populations that rapidly transitioned between open and closed states were influenced by voltage (Figure S8b-iv, Supporting Information). Strikingly, the probability of the pore to be in an open state (P_O) was heavily influenced by voltage (Figures S11 and S12, Supporting Information). As voltages increased from +20 to +100 mV the open probability drastically decreased from 0.99 to 0.12, respectively, with a transition from a mostly open state to a mostly closed state $\approx$ +50 mV (Figures S11 and S12, Supporting Information). This data suggest that the nanomechanical pore can be used as a voltage sensor.

The affinity for protein recognition was then tested using a PMP-2 pore containing biotin tags at adjacent corners (**Figure 4**). For electrical recording analysis, the pore had not been incubated with streptavidin. In the single-channel current traces at +80 mV, pore populations showed rapid transitions between open and closed states (Figure 4a-ii), similar to the PMP-0 pore (Figure S8b-iv, Supporting Information). To a rapidly gating PMP-2 pore, streptavidin was added and gating monitored. After the addition, the occurence of gating events decreased drastically (Figure 4b-ii).

In terms of open probabilities, the protein pore before protein addition had a P_O value of 0.22 (Figure 4a-iii), which increased to 0.98 upon protein addition (final concentration of 33 nM streptavidin)(Figure 4b-iii). Hence, streptavidin binding to the biotin-pore stabilizes the pore structure, as found for the PMP-2 pore pre-incubated with protein. Through analysis of pore open probabilities, this data provides a method for target-specific protein detection using a mechanical DNA nanopore.

3. Conclusion

We have pioneered the rational design of large diameter membrane nanopores with controlled nanoscale mechanical transitions. The stimulus-actuated nanopores have been inspired by biological ion channels and other proteins that undergo mechanical changes to fulfil their functions.[72,73] To replicate nanoscale transitions via synthetic routes, the 10 nm-wide DNA nanopore structures were designed to dynamically switch in pore shape but undergo stabilization by either DNA hybridization or protein binding. Previous large DNA nanopores were static in their lumen shape[41,42] and one design featured a flap to close or open the pore lumen of fixed dimensions.[42] By changing the entire shape, our designer pores advance typical ligand-gated ion channels that have a less tunable range of activators as well as much narrower lumens. Our DNA pores differ in other ways from biological templates as the latter reversibly dissociate ligands when switching back to the other pore conformation. Furthermore, several biological ion channels completely close the lumen for transport. In future, these two aspects may be integrated into the DNA nanopore with design changes that harness DNA nanotechnology. Further developments may also include selectivity filters for cargo-specific transport, something which

is shown with stimuli-responsive and biomimetic channels fabricated in solid-state membranes that, however, do not undergo conformational changes in the pore structure.[74–76] As our DNA designer pores can insert into semifluid membranes, applications are opened for applications compatible with synthetic polymer films.[77] The inherent design freedom may also enable the exploitation of the nanomechanical pores for controlled transport of bioactive cargos into biological cells, the construction of cell-cell communication for artificial gap junctions,[78] the formation of synthetic cells that are environmentally responsive by permeabilizing their membranes, or controlled drug release. In conclusion, by mimicking and expanding biological ion channels using designer DNA-origami structures, our study extends the scope and versatility of artificial nanopores for use in fundamental research and biosensing and biomedical applications.[79]

4. Experimental Section

Materials: All DNA oligonucleotides were purchased from Integrated DNA Technologies, except the 5′-cholesterol-labelled DNA oligonucleotide, which was ordered from Eurogentec. The M13 and phiX174 DNA scaffolds and restriction enzymes were ordered from New England Biolabs. All other reagents were purchased from Sigma–Aldrich unless stated otherwise.

Design of the DNA-Origami Structures: The DNA nanostructures were designed using caDNAno software.[80] The DNA design schemes for the mechanical caps and pores are provided in Figures S1 and S2 (Supporting Information). All sequences of DNA oligonucleotides are summarized in Table S1 (Supporting Information).

Preparation of the DNA Nanostructures: The assembly, gel purification, and TEM analysis of the DNA nanostructures followed protocols previously described.[71] To fold the DNA mechanical caps and pores, the restriction enzyme pre-treated M13 scaffold and the non-cut phiX174 scaffold, respectively, were mixed at a 1:5 ratio with corresponding staples in 0.5× TAE buffer supplemented with 16 mM MgCl$_2$. The DNA-origami structures were folded using a 40 h folding program: the solutions were first heated at 75 °C for 5 min to denature the scaffold and any folded staple strands, and then, for annealing, cooled from 65 to 25 °C at a rate of 1 °C h^{-1}, followed by cooling to 10 °C at a rate of 1 °C per 5 min. The samples were kept at 4 °C until further use. After the folding process, the DNA-origami structures were purified by excision from a 1.2% agarose gel run in 0.5x TBE buffer supplemented with 11 mM MgCl$_2$. The cholesterol-tagged pores were prepared by adding cholesterol-labeled strands to the purified pores at a stoichiometry of 1.5 relative to the total number of DNA cholesterol attachment sites on the DNA nanopores. It was essential that the cholesterol-tagged pores were freshly prepared and used for the current recording experiments on the same day.

Agarose Gel Electrophoresis Analysis of the DNA Nanostructures: The folded DNA caps and nanopores were analyzed using 1.5% agarose gel electrophoresis in 0.5× TBE buffer supplemented with 11 mM MgCl$_2$. Gels were run at 65 V in an ice–water bath for various hours depending on the samples.

TEM Characterization of the DNA Nanostructures: Purified DNA nanostructures (6 μL) were added onto TEM grids treated by glow discharge (Agar Scientific, AGG2050C) and then stained with 2% uranyl formate solution, as described.[71] The samples were analyzed on a JEM-2100 electron microscope operated at 200 kV and the images were acquired with an Orius SC200 camera. TEM images of the rhombus-shaped DNA nanostructures were subjected to ImageJ analysis to measure the dimensions and the smallest angle between the subunits of the pore.

Single-Channel Current Recordings: For planar lipid bilayer electrophysiological current measurements,[71] integrated chip-based, parallel bilayer recording setups (Orbit Mini; Nanion Technologies, Munich, Germany) with multielectrode-cavity-array (MECA) chips (IONERA, Freiburg,

Germany) were used.[65] Bilayers were formed of DPhPC lipid dissolved in octane (10 mg mL^{-1}). The electrolyte solution was 1 M KCl and 10 mM HEPES, pH 7.6. For pore insertion, a 2:1 DNA nanopore and 0.5% OPOE[81] (n-octyloligooxyethylene, in 1 M KCl, 10 mM HEPES, pH 7.6) was added to the cis chamber; the trans side was electrically grounded. Successful incorporation was observed by detecting current steps. Open and closed states were confirmed using all-point histograms. If currents clustered into two peaks on the histogram, each peak was individually analyzed to obtain average current and conductance measurements. Current traces were acquired at 20 kHz and subsequently Bessel-filtered, using Element Data Recorder software (Element s.r.l., Italy).

Supporting Information

Supporting Information is available from the Wiley Online Library or from the author.

Conflict of Interest

The nanopore technology has been licensed to Oxford Nanopore Technologies plc.

Data Availability Statement

The data that support the findings of this study are available from the corresponding author upon reasonable request.

[1] C. Lee, J. Guo, W. Zeng, S. Kim, J. She, C. Cang, D. Ren, Y. Jiang, *Nature* **2017**, *547*, 472.

[2] G. E. Flynn, J. P. Johnson, W. N. Zagotta, *Nat. Rev. Neurosci.* **2001**, *2*, 643.

[3] A. J. R. Plested, *Nat. Struct. Mol. Biol.* **2016**, *23*, 494.

[4] I. Gushchin, I. Melnikov, V. Polovinkin, A. Ishchenko, A. Yuzhakova, P. Buslaev, G. Bourenkov, S. Grudinin, E. Round, T. Balandin, V. Borshchevskiy, D. Willbold, G. Leonard, G. Büldt, A. Popov, V. Gordeliy, *Science* **2017**, *356*, 6342.

[5] G. Goodwin, S. B. McMahon, *Nat. Rev. Neurosci.* **2021**, *22*, 263.

[6] H. C. Lai, L. Y. Jan, *Nat. Rev. Neurosci.* **2006**, *7*, 548.

[7] G. Yellen, *Nature* **2002**, *419*, 35.

[8] E. Perozo, *Nat. Rev. Mol. Cell Biol.* **2006**, *7*, 109.

[9] J. M. Kefauver, A. B. Ward, A. Patapoutian, *Nature* **2020**, *587*, 567.

[10] I. R. Booth, M. D. Edwards, S. Black, U. Schumann, S. Miller, *Nat. Rev. Microbiol.* **2007**, *5*, 431.

**ADVANCED
SCIENCE NEWS**

www.advancedsciencenews.com

**ADVANCED
MATERIALS**

www.advmat.de

[11] V. Vásquez, M. Sotomayor, J. Cordero-Morales, K. Schulten, E. Perozo, *Science* **2008**, *321*, 1210.

[12] A. Kocer, *Curr. Opin. Chem. Biol.* **2015**, *29*, 120.

[13] W. A. Catterall, G. Wisedchaisri, N. Zheng, *Nat. Chem. Biol.* **2020**, *16*, 1314.

[14] J. Clarke, H.-C. Wu, L. Jayasinghe, A. Patel, S. Reid, H. Bayley, *Nat. Nanotechnol.* **2009**, *4*, 265.

[15] J. Quick, N. J. Loman, S. Duraffour, J. T. Simpson, E. Severi, L. Cowley, J. A. Bore, R. Koundouno, G. Dudas, A. Mikhail, N. Ouédraogo, B. Afrough, A. Bah, J. H. J. Baum, B. Becker-Ziaja, J. P. Boettcher, M. Cabeza-Cabrerizo, Á. Camino-Sánchez, L. L. Carter, J. Doerrbecker, T. Enkirch, I. G.- Dorival, N. Hetzelt, J. Hinzmann, T. Holm, L. E. Kafetzopoulou, M. Koropogui, A. Kosgey, E. Kuisma, C. H. Logue, et al., *Nature* **2016**, *530*, 228.

[16] M. Jain, S. Koren, K. H. Miga, J. Quick, A. C. Rand, T. A. Sasani, J. R. Tyson, A. D. Beggs, A. T. Dilthey, I. T. Fiddes, S. Malla, H. Marriott, T. Nieto, J. O'Grady, H. E. Olsen, B. S. Pedersen, A. Rhie, H. Richardson, A. R. Quinlan, T. P. Snutch, L. Tee, B. Paten, A. M. Phillippy, J. T. Simpson, N. J. Loman, M. Loose, *Nat. Biotechnol.* **2018**, *36*, 338.

[17] S. E. van der Verren, N. van Gerven, W. Jonckheere, R. Hambley, P. Singh, J. Kilgour, M. Jordan, E. J. Wallace, L. Jayasinghe, H. Remaut, *Nat. Biotechnol.* **2020**, *38*, 1415.

[18] P. Goyal, P. v. Krasteva, N. van Gerven, F. Gubellini, I. van den Broeck, A. Troupiotis-Tsaïlaki, W. Jonckheere, G. Péhau-Arnaudet, J. S. Pinkner, M. R. Chapman, S. J. Hultgren, S. Howorka, R. Fronzes, H. Remaut, *Nature* **2014**, *516*, 250.

[19] F. Rivas, O. K. Zahid, H. L. Reesink, B. T. Peal, A. J. Nixon, P. L. DeAngelis, A. Skardal, E. Rahbar, A. R. Hall, *Nat. Commun.* **2018**, *9*, 1037.

[20] X. Liu, M. M. Skanata, D. Stein, *Nat. Commun.* **2015**, *6*, 6222.

[21] R. Wei, V. Gatterdam, R. Wieneke, R. Tampé, U. Rant, *Nat. Nanotechnol.* **2012**, *7*, 257.

[22] G. Huang, A. Voet, G. Maglia, *Nat. Commun.* **2019**, *10*, 835.

[23] H. Ouldali, K. Sarthak, T. Ensslen, F. Piguet, P. Manivet, J. Pelta, J. C. Behrends, A. Aksimentiev, A. Oukhaled, *Nat. Biotechnol.* **2020**, *38*, 176.

[24] C. Cao, Y.-L. Ying, Z.-L. Hu, D.-F. Liao, H. Tian, Y.-T. Long, *Nat. Nanotechnol.* **2016**, *11*, 713.

[25] A. K. Thakur, L. Movileanu, *Nat. Biotechnol.* **2019**, *37*, 96.

[26] N. S. Galenkamp, A. Biesemans, G. Maglia, *Nat. Chem.* **2020**, *12*, 481.

[27] G. Wang, L. Wang, Y. Han, S. Zhou, X. Guan, *Acc. Chem. Res.* **2013**, *46*, 2867.

[28] D. H. Stoloff, M. Wanunu, *Curr. Opin. Biotechnol.* **2013**, *24*, 699.

[29] J. E. Reiner, A. Balijepalli, J. W. Robertson, J. Campbell, J. Suehle, J. J. Kasianowicz, *Chem. Rev.* **2012**, *112*, 6431.

[30] B. N. Miles, A. P. Ivanov, K. A. Wilson, F. Doğan, D. Japrung, J. B. Edel, *Chem. Soc. Rev.* **2013**, *42*, 15.

[31] S. Howorka, *Nat. Nanotechnol.* **2017**, *12*, 619.

[32] L. Restrepo-Pérez, C. Joo, C. Dekker, *Nat. Nanotechnol.* **2018**, *13*, 786.

[33] S. Zeng, C. Wen, P. Solomon, S.-L. Zhang, Z. Zhang, *Nat. Nanotechnol.* **2019**, *14*, 1056.

[34] D. Qiao, Y. Chen, H. J. Tan, R. H. Zhou, J. D. Feng, *Sci. China: Chem.* **2022**, *65*, 2122.

[35] C. Xu, P. Lu, T. M. Gamal El-Din, X. Y. Pei, M. C. Johnson, A. Uyeda, M. J. Bick, Q. Xu, D. Jiang, H. Bai, G. Reggiano, Y. Hsia, T. J. Brunette, J. Dou, D. Ma, E. M. Lynch, S. E. Boyken, P.-S. Huang, L. Stewart, F. DiMaio, J. M. Kollman, B. F. Luisi, T. Matsuura, W. A. Catterall, D. Baker, *Nature* **2020**, *585*, 129.

[36] K. R. Mahendran, A. Niitsu, L. Kong, A. R. Thomson, R. B. Sessions, D. N. Woolfson, H. Bayley, *Nat. Chem.* **2017**, *9*, 411.

[37] N. H. Joh, T. Wang, M. P. Bhate, R. Acharya, Y. Wu, M. Grabe, M. Hong, G. Grigoryan, W. F. DeGrado, *Science* **2014**, *346*, 1520.

[38] P. Lu, D. Min, F. DiMaio, K. Y. Wei, M. D. Vahey, S. E. Boyken, Z. Chen, J. A. Fallas, G. Ueda, W. Sheffler, V. K. Mulligan, W. Xu, J. U. Bowie, D. Baker, *Science* **2018**, *359*, 1042.

[39] A. Henning-Knechtel, J. Knechtel, M. Magzoub, *Nucleic Acids Res.* **2017**, *45*, 12057.

[40] E. Spruijt, S. E. Tusk, H. Bayley, *Nat. Nanotechnol.* **2018**, *13*, 739.

[41] Y. Xing, A. Dorey, L. Jayasinghe, S. Howorka, *Nat. Nanotechnol.* **2022**, *17*, 708.

[42] S. Dey, A. Dorey, L. Abraham, Y. Xing, I. Zhang, F. Zhang, S. Howorka, H. Yan, *Nat. Commun.* **2022**, *13*, 2271.

[43] N. C. Seeman, H. F. Sleiman, *Nat. Rev. Mater.* **2017**, *3*, 17068.

[44] F. Hong, F. Zhang, Y. Liu, H. Yan, *Chem. Rev.* **2017**, *117*, 12584.

[45] S. Nummelin, J. Kommeri, M. A. Kostiainen, V. Linko, *Adv. Mater.* **2018**, *30*, 1703721.

[46] Y. Hu, C. M. Niemeyer, *Adv. Mater.* **2019**, *31*, 1806294.

[47] P. W. K. Rothemund, *Nature* **2006**, *440*, 297.

[48] S. M. Douglas, H. Dietz, T. Liedl, B. Högberg, F. Graf, W. M. Shih, *Nature* **2009**, *459*, 414.

[49] Y. Ke, L. L. Ong, W. M. Shih, P. Yin, *Science* **2012**, *338*, 1177.

[50] E. Benson, A. Mohammed, J. Gardell, S. Masich, E. Czeizler, P. Orponen, B. Högberg, *Nature* **2015**, *523*, 441.

[51] H. Dietz, S. M. Douglas, W. M. Shih, *Science* **2009**, *325*, 725.

[52] D. Han, S. Pal, J. Nangreave, Z. Deng, Y. Liu, H. Yan, *Science* **2011**, *332*, 342.

[53] T. Liedl, B. Högberg, J. Tytell, D. E. Ingber, W. M. Shih, *Nat. Nanotechnol.* **2010**, *5*, 520.

[54] A. E. Marras, L. Zhou, H. J. Su, C. E. Castro, *Proc. Natl. Acad. Sci. USA* **2015**, *112*, 713.

[55] J. Ji, D. Karna, H. Mao, *Chem. Soc. Rev.* **2021**, *50*, 11966.

[56] F. N. Gür, S. Kempter, F. Schueder, C. Sikeler, M. J. Urban, R. Jungmann, P. C. Nickels, T. Liedl, *Adv. Mater.* **2021**, *33*, 2101986.

[57] M. Shahhosseini, A. Kucinic, P. Beshay, W. Pfeifer, C. Castro, in *DNA Origami: Structures, Technology, and Applications*, Wiley, Hoboken, NJ, USA **2022**, pp. 101–133.

[58] A. Kuzyk, R. Schreiber, Z. Fan, G. Pardatscher, E.-M. Roller, A. Högele, F. C. Simmel, A. O. Govorov, T. Liedl, *Nature* **2012**, *483*, 311.

[59] Y. Yang, J. Wang, H. Shigematsu, W. Xu, W. M. Shih, J. E. Rothman, C. Lin, *Nat. Chem.* **2016**, *8*, 476.

[60] M. Langecker, V. Arnaut, T. G. Martin, J. List, S. Renner, M. Mayer, H. Dietz, F. C. Simmel, *Science* **2012**, *338*, 932.

[61] J. R. Burns, E. Stulz, S. Howorka, *Nano Lett.* **2013**, *13*, 2351.

[62] J. R. Burns, A. Seifert, N. Fertig, S. Howorka, *Nat. Nanotechnol.* **2016**, *11*, 152.

[63] K. Göpfrich, C.-Y. Li, M. Ricci, S. P. Bhamidimarri, J. Yoo, B. Gyenes, A. Ohmann, M. Winterhalter, A. Aksimentiev, U. F. Keyser, *ACS Nano* **2016**, *10*, 8207.

[64] S. Krishnan, D. Ziegler, V. Arnaut, T. G. Martin, K. Kapsner, K. Henneberg, A. R. Bausch, H. Dietz, F. C. Simmel, *Nat. Commun.* **2016**, *7*, 12787.

[65] T. Diederichs, G. Pugh, A. Dorey, Y. Xing, J. R. Burns, Q. H. Nguyen, M. Tornow, R. Tampé, S. Howorka, *Nat. Commun.* **2019**, *10*, 5018.

[66] R. P. Thomsen, M. G. Malle, A. H. Okholm, S. Krishnan, S. S.-R. Bohr, R. S. Sørensen, O. Ries, S. Vogel, F. C. Simmel, N. S. Hatzakis, J. Kjems, *Nat. Commun.* **2019**, *10*, 5655.

[67] P. M. Arnott, S. Howorka, *ACS Nano* **2019**, *13*, 3334.

[68] C. Lanphere, P. M. Arnott, S. F. Jones, K. Korlova, S. Howorka, *Angew. Chem., Int. Ed.* **2021**, *60*, 1903.

[69] D. Offenbartl-Stiegert, A. Rottensteiner, A. Dorey, S. Howorka, *Angew. Chem., Int. Ed.* **2022**, *61*, e202210886.

[70] A. Seifert, K. Göpfrich, J. R. Burns, N. Fertig, U. F. Keyser, S. Howorka, *ACS Nano* **2015**, *9*, 1117.

[71] C. Lanphere, D. Offenbartl-Stiegert, A. Dorey, G. Pugh, E. Georgiou, Y. Xing, J. R. Burns, S. Howorka, *Nat. Protoc.* **2021**, *16*, 86.

[72] A. Goel, V. Vogel, *Nat. Nanotechnol.* **2008**, *3*, 465.

[73] A. E. M. Beedle, S. Garcia-Manyes, *Nat. Rev. Mater.* **2022**, *8*, 10.

[74] J. R. Basore, N. v. Lavrik, L. A. Baker, *Adv. Mater.* **2010**, *22*, 2759.

[75] X. Hou, W. Guo, L. Jiang, *Chem. Soc. Rev.* **2011**, *40*, 2385.

[76] Q. Liu, L. Wen, K. Xiao, H. Lu, Z. Zhang, G. Xie, X.-Y. Kong, Z. Bo, L. Jiang, *Adv. Mater.* **2016**, *28*, 3181.

[77] J. R. Sanborn, X. Chen, Y. Yao, J. A. Hammons, R. H. Tunuguntla, Y. Zhang, C. C. Newcomb, J. A. Soltis, J. J. Yoreo, A. Buuren, A. N. Parikh, A. Noy, *Adv. Mater.* **2018**, *30*, 1803355.

[78] S. Mantri, K. Tanuj Sapra, S. Cheley, T. H. Sharp, H. Bayley, *Nat. Commun.* **2013**, *4*, 1725.

[79] J.-B. Fan, Y. Li, S. Wang, L. Jiang, in *Nanomedicine: Micro/Nano Technologies* (Ed.: N. Gu), Springer, Singapore **2023**, pp. 19–48.

[80] S. M. Douglas, A. H. Marblestone, S. Teerapittayanon, A. Vazquez, G. M. Church, W. M. Shih, *Nucleic Acids Res.* **2009**, *37*, 5001.

[81] D. Morzy, M. Schaich, U. F. Keyser, *Molecules* **2022**, *27*, 578.